This article has been accepted for publication in a future issue of this journal, but has not been fully edited. Content may change prior to final publication. Citation information: DOI 10.1109/TCSVT.2016.2615444, IEEE Transactions on Circuits and Systems for Video Technology

Structure-adaptive Fuzzy Estimation for Random-Valued Impulse Noise Suppression

Yang Chen, *Member, IEEE*, Jian Yang, Yudong Zhang, Huazhong Shu, *Senior Member*, *IEEE*, Limin Luo*, Senior Member*, *IEEE*, Jean-Louis Coatrieux, *Fellow*, *IEEE,* and Qianjing Feng

***Abstract*—Noise detection accuracy is crucial in suppressing random-valued impulse noise. Both false and miss detections determine the final estimation performance. Deterministic detection methods, which distinctly classify pixels into noisy or uncorrupted pixels, tend to increase the estimation error because some uncorrupted edge points are hard to discriminate from the random-valued impulse noise points. This paper proposes an iterative Structure-adaptive Fuzzy Estimation (SAFE) for random-valued impulse noise suppression. This SAFE method is developed in the framework of Gaussian Maximum Likelihood Estimation (GMLE). The structure-adaptive fuzziness is reflected by two structure-adaptive metrics based on pixel reliability and patch similarity, respectively. The reliability metric for each pixel (as noise free) is estimated via a novel Minimal Path Based Structure Propagation (MPSP) to give full consideration of the spatially varying image structures. A robust iteration stopping strategy is also proposed by evaluating the re-estimation error of the uncorrupted intensity information. Comparative experiment results show that the proposed structure-adaptive fuzziness can lead to effective restoration. Efficient implementation of this SAFE method is also realized via GPU (Graphic Processing Unit)-based parallelization.**

***Index Terms*—Random-valued impulse noise, Structure-adaptive Fuzzy Estimation (SAFE), reliability metric, similarity metric.**

I. INTRODUCTION

IN signal acquisition or transmission, observed images are often corrupted by impulse noise arising from sensor damage, malfunctioning or timing errors, faulty memory locations in hardware or bit errors [1-2]. When images are corrupted by impulse noise, the intensities of some pixels are changed to some wrong values, which often lead to high-contrast artifacts in the image. It is thus necessary to remove the impulse noise to guarantee a good performance of subsequent image processes such as edge detection, image segmentation and object tracking.

Let I_{ij} be the pixel intensity of an image I at location (*i, j*), and $\left[I_{\min}, I_{\max}\right]$ be the dynamic intensity range of I. With x_{ij} denoting the intensity of the corresponding noisy image at location (*i,j*), then

$$x_{ij}=\begin{cases} n_{ij} & \text{with probability } \rho \\ I_{ij} & \text{with probability 1-}\rho \end{cases} \tag{1}$$

where $n_{ij} \in \left[I_{\min}, I_{\max}\right]$ is the value of corrupted points and ρ denotes the noise density or ratio. Here, for fixed-valued "salt-and-pepper" noise, noisy pixels n_{ij} take either $I_{\min}$ or $I_{\max}$ values [3-9]. As to the random-valued impulse noise, noisy pixels x_{ij} can take any random value between $I_{\min}$ and $I_{\max}$. Compared to random-valued impulse noise, salt-and-pepper noise is much easier to identify, remove and restore via target-specific operations on corrupted points.

Many filters have been proposed to suppress random-valued impulse noise in the past twenty years. It is well accepted that the performance of filtering is highly dependent on the detection precision of corrupted points. In [10], Chen and Wu proposed an adaptive center-weighted median filter (ACWMF) with a switching scheme based on an impulse detection mechanism, which was then combined with a detail-preserving regularization and a sparse representation [11-13]. In [14], a noise detection method according to the minimum absolute value of four convolutions was proposed. In [15], Aizenberg et al. developed two noise detectors called differential rank impulse detector (DRID) and enhanced rank impulse detector (ERID). And in [16], Garnett et al. exploited the rank-ordered absolute differences (ROAD) statistic to develop bilateral filtering for impulse noise suppression. In [17] and [18], Dong et al. improved the detection of ROAD by using a logarithmic function and a directional weighting strategy, respectively. Then, in [19], a rank-ordered relative difference (RORD) statistic impulse detector was proposed in a recursive weighted mean filter for the removal of random-valued impulse noise. In

This work was supported in part by the National Natural Science Foundation under Grants 81370040, 81530060, in part by the Fundamental Research Funds for the Central Universities, and the Qing Lan Project in Jiangsu Province.

Y. Chen, H. Shu, and L. Luo are with the Laboratory of Image Science and Technology, Southeast University, Nanjing 210096, China, also with the Centre de Recherche en Information Biomedicale Sino-Francais, Rennes F-35000, France, and also with the Key Laboratory of Computer Network and Information Integration, Ministry of Education, Southeast University, Nanjing 210096, China (e-mail: chenyang.list@seu.edu.cn; shu.list@seu.edu.cn; luo.list@seu.edu.cn).

J. Yang is with the Beijing Engineering Research Center of Mixed Reality and Advanced Display, School of Optics and Electronics, Beijing Institute of Technology, Beijing 100081, China (e-mail: jyang@bit.edu.cn).

Y. Zhang is with the School of Computer Science and Technology, Nanjing Normal University, Nanjing 210097, China (e-mail: zhangyudong @njnu.edu.cn).

J.-L. Coatrieux is with the Centre de Recherche en Information Biomedicalee Sino-Francais, Rennes 35042, France, also with the National Institute for Health and Medical Research, Rennes F-35000, France, and also with the Laboratoire Traitement du Signal et de l'Image, Université de Rennes 1, Rennes F-35000, France (e-mail: jean-louis.coatrieux@univ-rennes1.fr).

Q. Feng is with Department of Biomedical Engineering, Southern Medical University, Guangzhou 510515, China (e-mail: fengqj99@fimmu.com).

This article has been accepted for publication in a future issue of this journal, but has not been fully edited. Content may change prior to final publication. Citation information: DOI 10.1109/TCSVT.2016.2615444, IEEE Transactions on Circuits and Systems for Video Technology

[20], a detection method based on directional intensity difference was proposed and used in an adaptive weighted mean filter. In [21], a filter named adaptive switching median (ASWM) with an automatically calculated threshold was reported for random-valued noise suppression. In [22], Wu and Tang proposed a new selective degenerate diffusion (NSDD) model for random-valued noise, in which pixels were classified into edge pixels, noisy pixels, and interior pixels, from which a controlling speed function was designed to adaptively suppress noise. Yan applied an adaptive outlier pursuit based method (AOP) in [23] to inpaint those points corrupted by random-valued noise.

In the case of random-valued impulse noise, noise pixels take arbitrary values within a dynamic range, which makes their detection challenging especially in regions with large intensity variations. Deterministic discrimination of noise points tends to greatly increase the estimation error. Recently, fuzzy techniques have been considered to improve filtering by exploiting a fuzzy characterization of the random-valued impulse noise. Several fuzzy type filters were proposed for fixed-valued impulse noise ([24-28]). Luo et al. [29] applied a trimmed mean based fuzzy detection method for random-valued impulse noise, from which a linear membership was calculated in order to get an improved edge-preserving filtering. In [30], a fuzzy reasoning-based directional median filter was devised by exploiting the directional information of intensity continuity. Schulte et al. [31] proposed a fuzzy noise detection and reduction method (FIDRM) for random-valued noise. Then, in [32], Schulte et al. extended the FIDRM method by detecting random-valued impulse noise points using directional gradient based fuzzy rules. Directional gradient information was also used in [33] as the input of a fuzzy system, the outputs being further submitted to a classification process to guide the restoration. In [34] and [35], a peer group concept was utilized in building fuzzy metrics for impulse noise detection. In [36], a decision-based fuzzy approach (DFA) relying on evidence theory was proposed for random-valued noise reduction. In [37], a fuzzy weighted non-local means (FWNLM) filter was developed to suppress random-valued noise.

In most of the above algorithms on random-valued impulse noise suppression, gradient information along some pre-fixed directions is calculated in order to avoid detecting some edge points as noise points. Nevertheless, we should also note that such fixed-directional constraints are inherently ineffective in reflecting the real image structures where varying intensities and orientations cannot be predicted. To overcome this, we propose a Structure-adaptive Fuzzy Estimation (SAFE) method to remove random-valued impulse noise in the framework of Gaussian Maximum Likelihood Estimation (GMLE). Spatially varying structure information is incorporated into this SAFE algorithm as the fuzziness metrics in the form of point reliability and structure similarity. Especially, a membership function evaluating the pixel-wise reliability is built via a novel Minimal Path Based Structure Propagation (MPSP) to capture the spatially varying structures in the image. An effective iteration stopping strategy is also proposed based on the error evaluation of the re-estimated un-corrupted information. The SAFE solution is implemented via GPU (Graphic Processing Unit)-based parallelization techniques. Numerical experiments conducted on different noise densities have been performed to assess the performance of the proposed algorithm.

The rest of this paper is organized as follows: in section II, we first give a short review of the Gaussian Maximum Likelihood Estimation (GMLE) in impulse noise suppression and its relationship with median filtering. Then, we describe the proposed SAFE algorithm and we detail both the minimal path based reliability metric and the re-estimation based iteration stopping criterion. Experimental results are given and discussed in section IV. Section V concludes this paper with a brief description of its contributions and some open issues for future work.

II. The Structure Adaptive Fuzzy Estimation (SAFE)

A. Structure Adaptive Fuzzy Estimation (SAFE)

As the most widely used methods in impulse noise suppression, median type filters estimate the corrupted pixel intensities as the medians of the neighboring intensities. The median operation corresponds to the maximum likelihood estimators of independent and identically distributed (i.i.d.) observations which obey Laplacian distributions with probability density function (pdf, denoted by f here) [38], [39]. Let $x_1,....,x_N$ be N i.i.d. Laplacian distributed observations with unknown location parameter μ and the same scale parameter η (deviation) from μ, the following Laplacian likelihood function of μ can be expressed by:

$$L(x_1,....,x_N;\mu)=\prod_{i=1}^{N} f(x_i-\mu)=\left(\frac{1}{2\eta}\right)^N \exp\left(-\mathrm{U}(x_i,\mu)/\eta\right) \quad (2)$$

$$\mathrm{U}(x_i,\mu)=\sum_{i=1}^{N}|x_i-\mu| \quad (3)$$

Maximizing Eq. (2) leads to the solution of the simple median $\hat{\mu}$ = MEDIAN$\left(x_1,....,x_N\right)$ [39]. Assuming the Laplacian distribution of the observations in a 3×3 window, 2D median filtering of center pixel value μ is in fact the maximization of the function (2) with respect to μ [40]. Likewise, with the assumption of Gaussian distribution, we can build the likelihood function:

$$\begin{aligned} L(x_1,....,x_N;\mu)&=\prod_{i=1}^{N} f(x_i-\mu) \\ &=\left(\frac{1}{2\pi\sigma^2}\right)^{N/2} \exp\left(-\sum_{i=1}^{N}(x_i-\mu)^2/2\sigma^2\right) \end{aligned} \quad (4)$$

Similarly, maximizing Eq.(4) on μ leads to Gaussian Maximum Likelihood Estimation (GMLE) as an averaging filtering operation.:

$$\hat{\mu}=\sum_{i=1}^{N} x_i \Big/ N \quad (5)$$

The variance of the estimated $\hat{\mu}$ is σ^2/N, which shows that the variance for GMLE decreases linearly as the number of

This article has been accepted for publication in a future issue of this journal, but has not been fully edited. Content may change prior to final publication. Citation information: DOI 10.1109/TCSVT.2016.2615444, IEEE Transactions on Circuits and Systems for Video Technology

observations increases. It was pointed out in [41] that such Gaussian distribution based averaging filtering can lead to better Pepper-Salt noise suppression than the Laplacian distribution based median filtering. However, assuming an identical variance assumption for all the samples, the averaging filtering Eq. (5) tends to smear image details. In fact, in estimating the points corrupted by random-valued impulse noise, neighboring points should not be assigned the same variance for the following two reasons ***A1*** and ***A2***:

A1: it is actually impossible to explicitly detect all the impulse noise points with no error because of the uncertainty caused by the random noise values and the spatially varying edge intensities. A fuzzy metric should be used to cope with this randomness, in which each pixel should be given a reliability value (between 0 and 1) to evaluate its probability of being an uncorrupted point. That is, following Eq. (4), those neighboring pixels with a high probability to be an impulse noise point should be trusted less and assigned a large variance.

***A2*:** neighboring pixels belonging to the structure similar to the current point should be considered with a higher probability of belonging to the same structure, and should be assigned a low variance in estimating the current pixel in Eq. (4). Thus, another fuzzy metric value from 0 to 1 can be used to reflect the similarity degree (from low to high) for neighboring pixels.

We can see that the term $2\sigma^2$ determines the contribution of the neighboring points in the estimation of the current pixel. So, based on ***A1*** and ***A2***, we can extend the identical variance strategy to an adaptive variance strategy. This option features the proposed Structure Adaptive Fuzzy Estimation (SAFE) for random-valued impulse noise suppression. An improved GMLE model can be obtained by replacing the identical variance term σ^2 in Eq. (4) by an adaptive variance term σ_{ij}^2, which is calculated as the reciprocal of the multiplication of the two fuzzy membership functions for the reliability and similarity metrics (r_{ij} and s_{ij}) of the neighboring point intensity x_{ij}. Denoting the noisy image and the target restored image by x and μ, we obtain the following improved likelihood function:

$$\begin{aligned} L\left(x_{1j},....,x_{Nj};\mu_j\right) &= \prod_{ij\in N_j} f\left(x_{ij}\text{-}\mu_j\right) \\ &= \left(\frac{1}{2\pi\sigma_{ij}^2}\right)^{|N_j|/2} \exp\left(r_j^{\mu}\left(\mu_j\text{-}x_j\right)^2\text{-}\left(1\text{-}r_j^{\mu}\right)\sum_{ij\in N_j}\left(x_{ij}\text{-}\mu_j\right)^2/2\sigma_{ij}^2\right) \\ &= \left(\frac{r_{ij}s_{ij}}{2\pi}\right)^{|N_j|/2} \exp\left(r_j^{\mu}\left(\mu_j\text{-}x_j\right)^2\text{-}\left(1\text{-}r_j^{\mu}\right)\sum_{ij\in N_j}\left(2r_{ij}s_{ij}\right)\left(x_{ij}\text{-}\mu_j\right)^2\right) \end{aligned} \quad (6)$$

Here, the subscripts in x_j and x_{ij} represent the intensities at point j and the points in its surrounding filter window N_j, respectively. Note that such subscript rule also applies to other notations in this paper. In Eq. (6), r_j^u and r_{ij} are the reliability metrics of the current point intensity x_j and its neighboring one x_{ij}. $|N_j|$ denotes the cardinal number of the filter window N_j. A detailed explanation of r_j^u, r_{ij} and s_{ij} is given as follows:

(a), $r_j^u \in [0,1]$ and $r_{ij} \in [0,1]$, and both take values from the same reliability map R. $r_j^u = 0$ means that pixel j is explicitly deemed as a corrupted noise point, and should be excluded in the GMLE function Eq. (6); $r_j^u = 1$ means that the pixel j is explicitly detected as an uncorrupted point, and in this case, the information of the neighbor pixels should be excluded in this GMLE function; r_{ij} is used to reflect the reliability degree of the neighbor pixel at ij in estimating μ_j.

(b), $s_{ij} \in (0,1)$ reflects the similarity degree between the current pixel j and its neighbor pixel ij. A smaller s_{ij} means that the neighbor pixel ij has a lower probability of belonging to the same structure containing the current pixel j, while a larger s_{ij} means that the pixel ij has a higher probability of belonging to the same structure. We use the "patch similarity" idea described in [42] to quantify the s_{ij} by an exponential function of ℓ^1 norm distance between neighboring patches [43-44]. Let P_j and P_{ij} be the two patches centered at pixel j and its neighbor pixel ij, the similarity metric s_{ij} is calculated via Eq. (7):

$$s_{ij} = \exp\left(-\left\|\mathrm{P}_{ij}^r\mathrm{P}_j^r\left(\mathrm{P}_{ij}-\mathrm{P}_j\right)\right\|_1/h\right) \quad (7)$$

Here, considering that the pixels with a lower reliability should be less weighted in the patch similarity calculation, we introduced two weighting patches P_{ij}^r and P_j^r storing the reliability value r for each points in P_{ij} and P_j (P_{ij} and P_j have the same size). The parameter h in (7) is used to modulate the exponent function value with respect to patch distance. Minimizing Eq. (6) with respect to μ_j leads to a linearly weighted solution:

$$\hat{\mu}_j = \frac{\left(r_j^{\mu}x_j + \left(1-r_j^{\mu}\right)\sum_{ij\in N_j/x_j}(r_{ij}s_{ij})x_{ij}\right)}{\left(r_j^{\mu} + \left(1-r_j^{\mu}\right)\sum_{ij\in N_j/x_j}(r_{ij}s_{ij})\right)} \quad (8)$$

B. Minimal Path Based Structure Propagation (MPSP) for Reliability Map Calculation

This article has been accepted for publication in a future issue of this journal, but has not been fully edited. Content may change prior to final publication. Citation information: DOI 10.1109/TCSVT.2016.2615444, IEEE Transactions on Circuits and Systems for Video Technology

For impulse noise point detection, intensity gradients along certain preset directions were widely used to discriminate edge points from noise points. But such calculations often fail to reflect the unpredictable inherent image structures. It is demonstrated in [45-47] that minimal path tracking can be applied to retrieve inherent image structures as the minimal path connection between two different points. So, we apply a Minimal Path based Structure Propagation (MPSP) approach to capture the spatially-varying feature information for noise point estimation. The proposed MPSP method is a minimal path tracking with no end point, in which the start point is simply set at the center point in each propagation window. With the potential function calculated as the cumulated intensity differences between each reached points and the center point, the MPSP method proceeds until two of the four borders of a square propagation window N_j^{mp} are reached. The structures the center points belonging to can be represented by the two connected minimal paths back-traced from the two border points to the center pixel j in each propagation window.

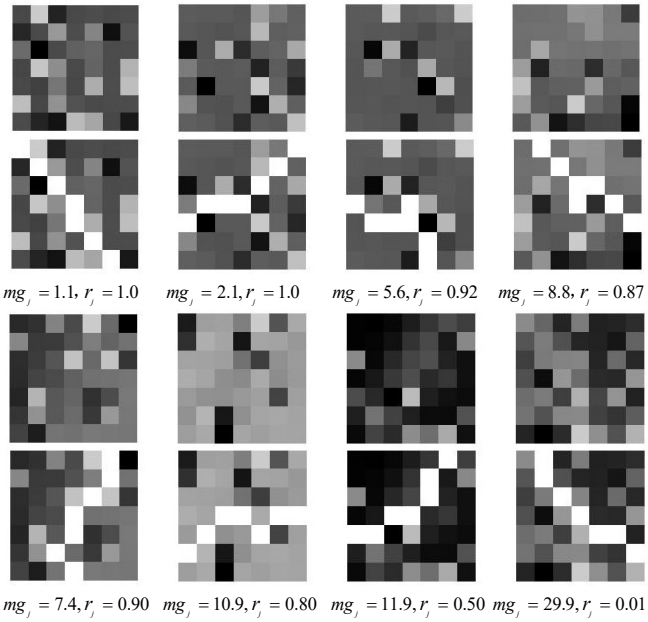

(a) The tracked minimal paths for eight uncorrupted points, which are the center points in the illustrated window images.

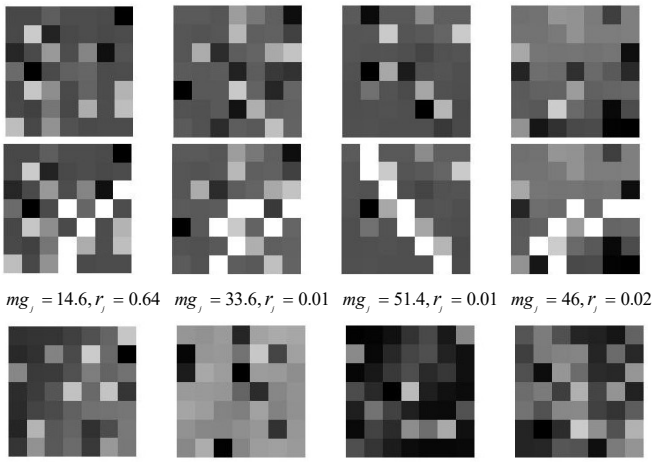

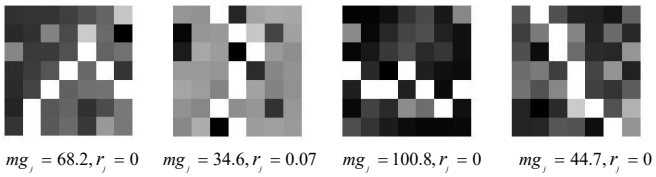

(b) The tracked minimal paths for eight corrupted points, which are the center points in the illustrated window images.

Fig.1. Illustration of the tracked minimal paths (in white color) for uncorrupted points. For both (a) and (b), the illustrations are presented in the forms of 7×7 propagation windows centered at the points to be considered. And the calculated mg values and reliability value r are listed below the corresponding pictures.

We illustrate in Fig.1(a) the tracked minimal paths for eight uncorrupted points, and Fig.1(b) the results for eight corrupted ones. These points were selected from the Lena image without and with 40% density of random-value impulse noise, and the illustrations are presented in 7×7 propagation windows centered at the points to be considered. For both Fig.1(a) and Fig.1(b), the first rows display the intensities in the original images. The second rows in Fig.1(a) and Fig.1(b) highlight the tracked minimal paths in white color, from which we can see that the tracked minimal paths take structure-preferable trajectories and can well avoid the corrupted points. For each center pixel j, we calculate the mean (denoted by mg_j) of the absolute values of intensity differences (with respect to the center pixel) for all the points in the back-traced minimal path L_j^{mp}. From the mg values in the captions below Fig.1(a) and (b), we can see that the random-valued impulse noise introduces abrupt intensity variations and tends to result in significantly larger mg values than the uncorrupted points. We can also find that some uncorrupted edge point (e.g. the right most column in Fig.1(a)) can even obtain larger mg values than some corrupted background points (e.g. the one in the left most column in Fig.1(b)).

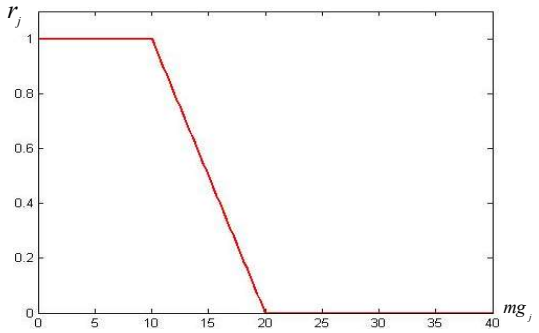

Fig.2. The fuzzy membership function for the reliability metric calculation.

Leveraging the fact that the mg values for most points often increase greatly after corruption, a pixel-wise fuzzy membership function is used to quantify the reliability degree for the pixels in map R. Fig.2 illustrates the fuzzy membership function (expressed in Eq. (10) below), with Lm_j and Hm_j denoting the two threshold parameters in calculating the fuzzy reliability for point j. As it can be seen in Fig.3, the points

This article has been accepted for publication in a future issue of this journal, but has not been fully edited. Content may change prior to final publication. Citation information: DOI 10.1109/TCSVT.2016.2615444, IEEE Transactions on Circuits and Systems for Video Technology

with mg_j values lower than Lm_j are distinctly considered as the originally uncorrupted points ($r_j = 1$) and the points with mg_j values larger than Hm_j are to be treated as noisy points ($r_j = 0$). For those points with mg_j values between Lm_j and Hm_j , a fuzzy value r_j between 0 and 1 is assigned to reflect the certainty degree of being uncorrupted. We plotted in Fig.3(a1), (b1), (c1) and (d1) the ordered *mg* values for the points in the four 7×7 propagation windows before (Fig.3(a2), (b2), (c2), (d2)) and after (Fig.3(a3), (b3), (c3), (d3)) noise corruption. Lena image with 40% density of random-value impulse noise is still used here. For each center pixel j , we calculate the mean (denoted by mg_j) of the absolute values of intensity differences (with respect to the center pixel) for the points in the back-traced minimal path L_j^{mp} . We can see that the *mg* values increase significantly after noise corruption, and a sharp increment of *mg* values can be easily noticed on the right side of each plot which corresponds to large *mg* values. We apply a K-means based clustering method to estimate the threshold parameters Lm_j and Hm_j . With an array N_j^{mg} storing the *mg* values in each propagation window N_j^{mp} , we classify all the *mg* values in N_j^{mp} into three data clusters LS_j^{mg} , LM_j^{mg} and LL_j^{mg} , corresponding respectively to the three sets of small, medium and large *mg* values:

$$\left[LS_j^{mg}, LM_j^{mg}, LL_j^{mg}, C_j^{mg} \right] = K\text{-}means(N_j^{mg}, 3) \quad (9)$$

Here, the K-means algorithm is chosen to cluster the data for its low complexity and is implemented based on the method reported in [48]. The "3" in the right part of Eq. (9) indicates that all the points in N_j^{mp} are clustered into three datasets based on their *mg* values. C_j^{mg} contains centroid mean values (C_{S-j}^{mg} , C_{M-j}^{mg} and C_{L-j}^{mg}) for respectively the three clusters (LS_j^{mg} , LM_j^{mg} and LL_j^{mg}). We should note that, due to the inherent intensity variations and the random values of noise points, some classification errors are inevitable with this K-means based clustering. In other words, some *mg* values from both corrupted and uncorrupted points might exist in all the three clusters. Also, by comparing the plots before and after corruption in Fig.3, we can understand that the sharp increments in the right parts of the plots were caused by the increased *mg* values due to noise corruption. So, in calculating the map R_j^N storing the reliability values for the points in N_j^{mp} ,we use the centroid values C_{S-j}^{mg} and C_{M-j}^{mg} as the threshold parameters Lm_j^{mp} and Hm_j^{mp} in Eq. (10) ($Lm_j^{mp} = C_{S-j}^{mg}$, $Hm_j^{mp} = C_{M-j}^{mg}$):

$$R_j^N = \begin{cases} 0 & mg_j > Lm_j \\ 1 - \left(mg_j \right) \Big/ \left(Hm_j^{mp} - Lm_j^{mp} \right) & Lm_j \le mg_j \le Hm_j \\ 1 & mg_j < Hm_j \end{cases} \quad (10)$$

In Eq. (10), mg_j stores the *mg* values for the points in N_j^{mp} . The points with mg_j values lower than Lm_j are distinctly considered as the originally uncorrupted points ($r_j = 1$) and the points with mg_j values larger than Hm_j are to be treated as noise points ($r_j = 0$). For those points with mg_j values between Lm_j and Hm_j , a fuzzy value r_j between 0 and 1 is assigned to reflect the certainty degree of being uncorrupted. We then extend each R_j^N to a larger map $\hat{R}_j^N$ of the same size as the input image (by setting the point values outside the N_j^{mp} to zero) and output the final fuzzy reliability map R (storing r_j values for all image points) by averaging all the $\hat{R}_j^N$ maps for all the j via Eq. (11):

$$R = \sum_j \hat{R}_j^N \Big/ \sum_j \hat{R}1_j^N \quad (11)$$

Here, $\hat{R}1_j^N$ denotes a unity map in the same size of $\hat{R}_j^N$, and is simply obtained by replacing the non-zero values in R_j^N by unity value. Now we can see that each reliability value r_j for pixel j is jointly determined by the distribution of all the *mg* values in the surrounding propagation window N_j^{mp} , which closely reflects local image structures. Just below the images in Fig.1(a) and Fig.1(b), we listed the calculated r_j values for different points: it is observed that the uncorrupted points have significantly larger r_j values than the corrupted ones.

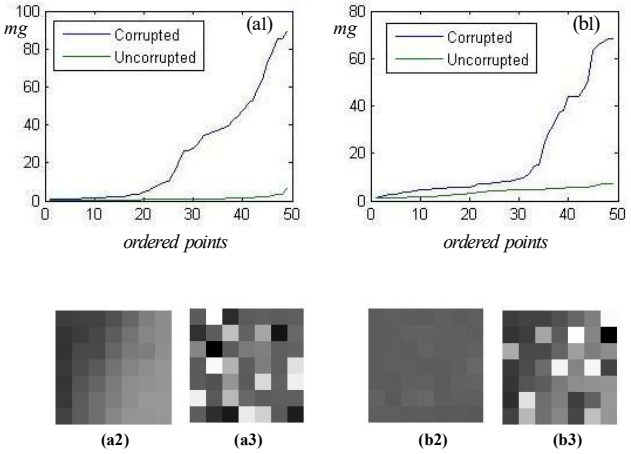

This article has been accepted for publication in a future issue of this journal, but has not been fully edited. Content may change prior to final publication. Citation information: DOI 10.1109/TCSVT.2016.2615444, IEEE Transactions on Circuits and Systems for Video Technology

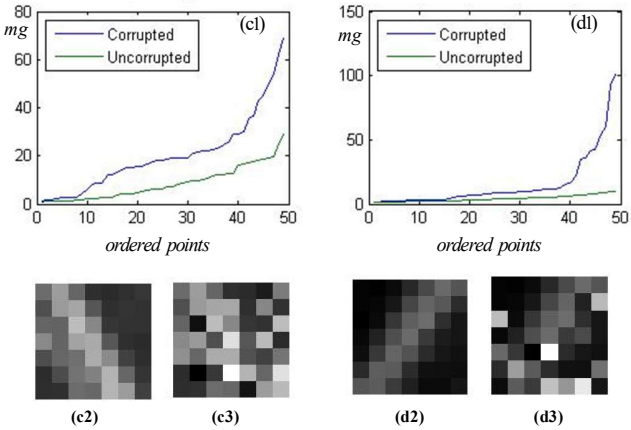

Fig.3. The ordered mg values of the points in propagation windows

Algorithm 1: The MPSP Algorithm

Initialization: set the size of each propagation window N_j^{mp} ;

Pixel-wise Loop (on each pixel index j):

1. Perform the minimal path propagation from current pixel j toward the direction with the minimal gradient magnitudes, and stop the propagation when two points lying in different borders are reached;
2. Retrieve the minimal path L_j^{mp} across the propagation window N_j^{mp} by back-tracing from the above two border points to the center pixel j ;
3. Calculate the mean mg_j of the intensity differences (with respect to the center pixel) for all the points in the back-traced minimal path L_j^{mp} .
4. Calculate the reliability map R that stores value r_j for each pixel j based on equations Eq. (9)-(11).

End Pixel-wise Loop

This MPSP algorithm is outlined above. One important merit of this MPSP method is its robustness in parameter setting because almost all the related parameters (e.g. propagation window size, threshold parameters, etc.) can be fixed in practical implementation.

C. Iteration Stopping Criterion Based on Pixel Re-estimation

Image quality will be improved after each restoration operation of Eq. (8). So, if we replace the input data x in Eqs. (6)-(8) by the updated image μ , a better restoration performance can be expected because the corrected intensities allow a more accurate calculation of the similarity metric s . However, over iterations, the benefits brought by this pixel correction will become more and more out-weighted by the negative effects caused by the inclusion of irrelevant pixels and the restored image quality will deteriorate if the iteration continues further. The ground truth image is not available to control the iteration number required to reach the optimal restoration. Therefore, the restoration deterioration is evaluated via a re-estimation strategy based on the assumption that the best restoration is reached when the surrounding intensities are able to provide the best estimation of the non-corrupted image information. After each iteration, we re-estimate the non-corrupted intensities via Eq. (12) using only the neighboring estimated intensities, the current pixel intensities being excluded. The non-corruption information for each pixel is thus introduced by the reliability metric r . We can obtain the re-estimated peak signal-to-noise ratio (PSNR-R) with respect to the non-corrupted image information via Eq. (12) and Eq. (13):

$$\mu_j^R = \sum_{ij \in N_j / x_j} (r_{ij} \cdot s_{ij}) \mu_{ij}^t \Big/ \sum_{ij \in N_j / x_j} (r_{ij} \cdot s_{ij}) \tag{12}$$

$$\text{PSNR-R}\left(t\right) = 10 \log_{10} \left(\text{Max}_I^{\,2} \Big/ \sum_{j=1}^{|M|} r_j \left(\mu_j^R - I_j \right)^2 \right) \tag{13}$$

where, $|M|$ and Max_I denote the pixel number and the maximum pixel intensity in the original image I , and t is the iteration index. The r_{ij} term in the summation operation in Eq. (12) is used to guarantee that only the uncorrupted information is used in PSNR-R calculation over iterations. The restored image is obtained when the PSNR-R starts to decrease. Though some estimation errors will be inevitably introduced due to the inaccuracy in calculating the reliability metric, it is found that this stopping strategy can well reflect the image deterioration for the cases with noise densities going from 10% up to 40%. When noise density increases over 40%, it is found that this strategy does not work because the increased noise density will increase error in the reliability metric estimation and greatly lower the estimation accuracy of the PSNR-R. So, in the case of noise density larger than 40%, we stop the iteration when the normed image difference between two consecutive iterations is less than a small ratio υ of the norm of the previous iterated image: $\|\mu^t - \mu^{t-1}\| / \|\mu^{t-1}\| < \upsilon$ ($\|\cdot\|$ is the ℓ^2 norm operator). Considering the fact that the knowledge of the exact noise density is not known, we perform a rough estimation of the overall noise density ρ_e using the calculated reliability value r_j stored in map R :

$$\rho_e = \sum_j \left(1 - r_j\right) \Big/ |M| \tag{14}$$

It is found that the estimated noise density range $\rho_e \in [32\%,\ 35\%]$ always provides a good map to the true noise density ρ=40% for all the images considered so far, so we use the estimated noise density ρ_e=35% to modulate the stopping strategy in the SAFE algorithm.

D. Outline of the SAFE Algorithm

The overall flowchart of the SAFE algorithm can be summarized as follows:

Algorithm 2: The SAFE Algorithm

1. Reliability map calculation and noise density estimation:

(1) Calculate the reliability map R based on the above MPSP method in Section B.

This article has been accepted for publication in a future issue of this journal, but has not been fully edited. Content may change prior to final publication. Citation information: DOI 10.1109/TCSVT.2016.2615444, IEEE Transactions on Circuits and Systems for Video Technology

(2) Calculate the estimated noise density ρ_e based on the reliability values in map R using Eq. (14).

2. Image restoration:

Initiate μ^0 to be the input image data x; set the size of the filter window N; Set ***StopIteration*** to FALSE; set t and $\mathrm{PSNR\_R}(1)$ to 1 and 0, respectively; set the ratio value υ (10^{-5} in this study).

While ***StopIteration*** = FALSE

Pixel-wise Loop (on pixel index j=1, 2, ... $|M|$):

Estimate the each pixel μ_j^t via Eq. (8);

Re-estimate each pixel μ_j^R via Eq. (12);

End Pixel-wise Loop

Calculate $\mathrm{PSNR\_R}(t)$ via Eq. (13);

If ($\mathrm{PSNR\_R}(t) < \mathrm{PSNR\_R}(t\text{-}1)$ **AND** $\rho_e <= 35\%$) **OR** ($\|\mu^t - \mu^{t-1}\| / \|\mu^{t-1}\| < \upsilon$ **AND** $\rho_e > 35\%$)

StopIteration = TRUE;

End

$t = t + 1$, and update x to μ^t;

End While

Output the image μ^t as the final restored image $\hat{\mu}$.

III. EXPERIMENTS

A. Experiment Configuration

Four grayscale images (Lena, Boat, Barbara and Peppers, referred under (a) to (d) in Fig.4) were chosen for the experiments. Random-value impulse noise with a density ranging from 20% to 60% (10% increments) is simulated. For comparison, the ACWMF(Adaptive Center-Weighted Median Filter), ROLD-EPR(Rank Ordered Logarithmic Difference based statistic combined with the Edge-Preserving Regularized method), DWM (Directional Weighted Median), ASWM (Adaptive Switching Median), RORD-WMF(Rank Ordered Relative Differences combined with Weighted Median Filter), NSDD (New Selective Degenerate diffusion), AOP (Adaptive Outlier Pursuit), DFA (decision-based fuzzy approach) and FWNLM (Fuzzy Weighted Non-Local Means) methods were implemented based on [10], [17], [18], [19,], [21], [22], [23], [36], [37], respectively.

Also, the parameters involved in these methods were suitably set based on their reference papers to obtain the best overall results in terms of PSNR (calculated via Eq. (22)) for all the four test images. The iterative ACWMF restoration approach applies four different groups of thresholds (Delta) in four center-weighted median operations, respectively. In the proposed SAFE method, we set the propagation window size to $PW = 7\times 7$, the cluster number $CN = 3$, the neighboring window size $NW = 17\times 17$, the patch size $PS = 9\times 9$, the smoothing parameter $h = 0.7$ and the ratio $\upsilon = 10^{-5}$. Here, $CN = 3$ was used because we need to cluster the points in the propagation window into small, medium and large *mg* values for the computation of the reliability values. Note that the parameter h modulates the relation between the similarity metric and the patch distance, and needs to be manually set to provide a satisfying restoration. The parameter values used in the other methods implemented for comparison purpose are defined in TABLE I.

The operations in Eq.(8)-Eq.(14) can be parallelized using the GPU based CUDA technique. Under the Compute Unified Device Architecture (CUDA) framework, we set the total number of blocks in grid to the row size of the image, and the total number of threads in each block to the column size of the image [49-50]. In implementing the SAFE algorithm, all the threads in the block-grid structure were executed in parallel to complete the involved pixel-wise operations. All the images were processed in a PC workstation (Intel Core™ 2 Quad CPU and 8192 Mb RAM, GPU (NVIDIA GTX475)) with Visual C++ as the developing environment (Visual Studio 2008 software; Microsoft). The restoration performance was quantitatively measured by the peak signal-to-noise ratio (PSNR) and the mean structural similarity index (MSSIM) proposed in [51]:

$$\mathrm{PSNR}(\hat{\mu}, I) = 10\log_{10}\left(|M| \cdot 255^2 \Big/ \sum_{j=1}^{|M|} (\hat{\mu}_j - I_j)^2 \right) \tag{15}$$

$$\mathrm{MSSIM}(\hat{\mu}, I) = \frac{\sum_{\Delta\hat{\mu}\in\hat{\mu}, \Delta I\in I} \frac{(2m_{\Delta\hat{\mu}} m_{\Delta I})(2\sigma_{\Delta\hat{\mu}\Delta I} + c_2)}{(m_{\Delta\hat{\mu}}^2 + m_{\Delta I}^2 + c_1)(\sigma_{\Delta\hat{\mu}}^2 + \sigma_{\Delta I}^2 + c_2)}}{|M|} \tag{16}$$

where, $\Delta\hat{\mu}$ and ΔI denote the 8×8 windows in the same position in the restored image $\hat{\mu}$ and the original true image I. $|M|$ is the total pixel number in the images. $m_{\Delta\hat{\mu}}$ and $m_{\Delta I}$ represent the mean intensities of $\Delta\hat{\mu}$ and ΔI, $\sigma_{\Delta\hat{\mu}}$ and $\sigma_{\Delta I}$ are the standard deviations of $\Delta\hat{\mu}$ and ΔI, $\sigma_{\Delta\hat{\mu}\Delta I}$ is the covariance of $\Delta\hat{\mu}$ and ΔI, $c_1 = (K_1 L)^2$ and $c_2 = (K_2 L)^2$ with L being the dynamic range of the pixel values (255 for 8-bit grayscale images). K_1 and K_2 are set to 0.01 and 0.03 as suggested in [51].

B. Restoration Results

Fig.5 to Fig.12 provide restoration results of the local ROI (regions of interest) cropped from the red rectangle regions in the test images in Fig.4. Fig.5 and Fig.6 correspond to the Lena image with 40% and 60% noise densities. Likewise, Fig.7 and Fig.8 present the results for the Boat image, Fig.9 and Fig.10 for the Barbara image, and Fig.11 and Fig.12 for the Peppers image. The calculated PSNR and MSSIM with respect to the original true images are given in the captions. In Fig.5-Fig.12, the original true images and the corrupted images are displayed in (a) and (b) for reference, and the restored images are shown in (c)-(h) for the methods ACWMF, ROLD-EPR, DWM, ASWM, RORD-WMF, NSDD, AOP, DFA, FWNLM, SAFE, respectively.

We can observe in Fig.5-Fig.12 that all the methods lead to noise suppression at some extent. It is also found that the restored images from ACWMF, ASWM, RORD-WMF, NSDD, AOP, and DFA methods are far from being satisfactory when

This article has been accepted for publication in a future issue of this journal, but has not been fully edited. Content may change prior to final publication. Citation information: DOI 10.1109/TCSVT.2016.2615444, IEEE Transactions on Circuits and Systems for Video Technology

TABLE I
PARAMETER SETTING FOR THE DIFFERENT METHODS

Methods	Parameter Settings
ACWMF	Delta=[100,85,70,65];Delta=[80, 65,50,45];Delta=[60, 45,30,25];Delta=[40, 25,10, 5];(Based on [10])
ROLD-EPR	$s=1.9, w=3\times3, m=4, for \quad p\le 25\%;\quad s=5.4, w=5\times5, m=12, for \quad p>25\%;$ $T_0=s\cdot q, T_{k+1}=T_k\cdot q(k\ge 0), K_{\max}=7, q$ is the number of pixel whose *ROLD* is less than s; (Based on[17])
DWMF	$w=5\times5, T_0=510, T_k=T_{k-1}\times0.8$,and iteration stops until the PSNR decreases ;(Based on [18])
ASWM	$w=3\times3, \alpha_0=20, \alpha_{n+1}=\alpha_n\times0.8(n\ge0), \varepsilon=0.01, \delta=0.1, iteration=6;$ (Based on[19])
RORD-WMF	$K_{\max}=2, m=4, FW=3\times3, RW=3\times3$ for noise ratio is less than 25%; $K_{\max}=3, m=10, FW=7\times7, RW=5\times5$ for noise ratio is higher than 25% (Based on[21])
NSDD	$W=5\times5, iternum=5, T=20$ for noise less than 30%; W=5×5 iternum=10,T=15 for noise ratio 40%; W=5×5,*iternum*=20,T=15 for noise ratio 50%;W=7×7,*iternum*=30,T=15 for noise ratio 60%; (Based on [22])
AOP	$\lambda=100, maxIter=7$ (Based on[23])
DFA	$W=3\times3; T=16$ for noise ratio 10% and 20%; $W=3\times3, T=18$ for noise ratio is higher than 20%; (Based on[36])
FWNLM	$SW=21\times21, MW=9\times9, T_1=380, T_2=120, h_\varepsilon=6;$ (Based on [37])
SAFE	$PW=7\times7, CN=3, NW=17\times17, PS=9\times9, h=0.7, \nu=10^{-5};$

noise density is high, with noise residuals clearly visible in Fig.6, Fig.8, Fig.10 and Fig.12 (60% noise density). Compared to these methods, the ROLD-EPR and DWM methods provide a better noise suppression but still suffer from blurring effects around some tiny structures. The FWNLM method improves the restoration quality by introducing a fuzzy weighting function into the non-local means filtering and presents an improved performance in noise suppression than other median-based filters. But oversmoothing effect can still be observed on some image details (see images (g) in Fig.5-Fig.12). With the fuzzy metrics utilizing both the pixel reliability information and patch similarity information, the SAFE algorithm leads to the best overall performance in terms of both noise suppression and detail preservation (see images (h) in Fig.5-Fig.12). Especially, we can see that some fine features (e. g. the hat structures in Lena image, the mast in Boat image, the scarf fabrics in Barbara image and the edges in the Pepper image) were better restored by the SAFE algorithm than by the other methods. High PSNR and MSSIM values are still obtained by the proposed SAFE method for 40% and 60% noise densities in Fig.5-Fig.12.

In Fig.13 and TABLE II, we summarize the PSNR and MSSIM values of the restored images for noise densities ranging from 20% to 60%. The highest values for different images and noise densities are given in bold numbers. We can observe in the plots that the PSNR and MSSIM values decrease as noise level rises in all cases. Overall, the proposed SAFE algorithm has the best performance in PSNR and MSSIM values among all the methods when noise density is higher than 20%, and this advantage becomes more prominent as noise density increases. The ACWMF method or RORD-WMF method leads in some cases to higher PSNR values than the SAFE method but the proposed SAFE method still behaves better in terms of MSSIM for most images. The FWNLM method provides higher PSNR or MSSIM values than the SAFE method for the Barbara image when the noise density is equal to 60%. However, even with a lower PSNR value than the FWNLM method (1.22% decrement from 23.10 to 22.82), the SAFE algorithm applied to the Barbara image (60% noise density) shows a much larger MSSIM improvement (7.19% increment from 0.7362 to 0.6868) over the FWNLM method.

Fig.4. The original test images. (a) Lena. (b) Boat. (c) Barbara. (d) Peppers. Note the red rectangles in the four images correspond to the zoomed local parts illustrated in Fig.5-Fig.12 below.

This article has been accepted for publication in a future issue of this journal, but has not been fully edited. Content may change prior to final publication. Citation information: DOI 10.1109/TCSVT.2016.2615444, IEEE Transactions on Circuits and Systems for Video Technology

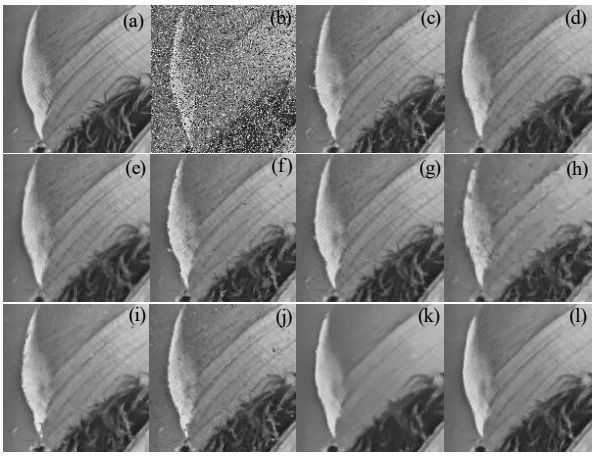

Fig.5. Restoration results for Lena image (40% noise density). (a) Original image; (b) Corrupted image; (c) ACWMF; (d) ROLD-EPR; (e) DWM; (f) ASWM;(g) RORD-WMF; (h) NSDD; (i) AOP; (j) DFA; (k) FWNLM; (l) SAFE.

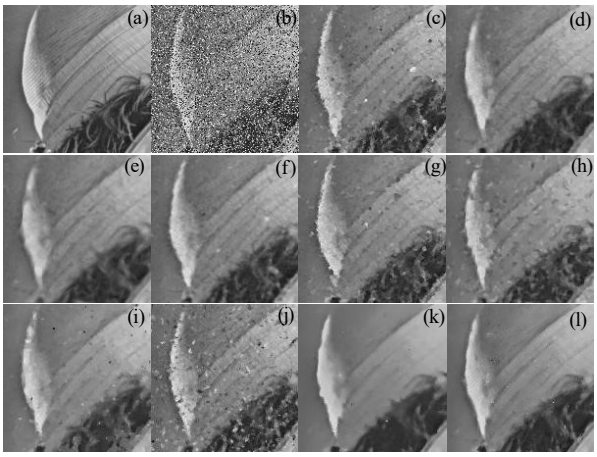

Fig.6. Restoration results for Lena image (60% noise density). (a) Original image; (b) Corrupted image; (c) ACWMF; (d) ROLD-EPR; (e) DWM; (f) ASWM;(g) RORD-WMF; (h) NSDD; (i) AOP; (j) DFA; (k) FWNLM; (l) SAFE.

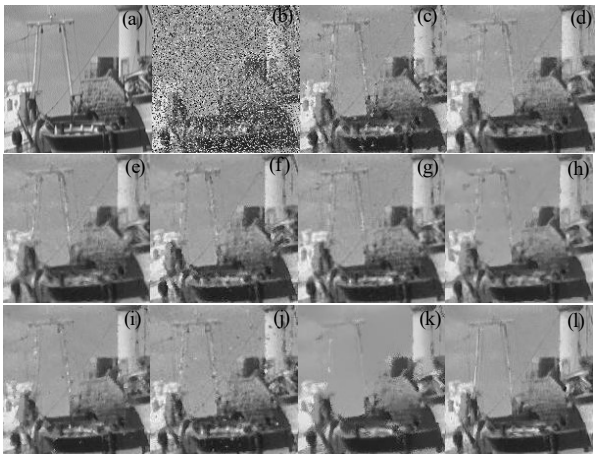

Fig.7. Restoration results for Boat image (40% noise density). (a) Original image; (b) Corrupted image; (c) ACWMF; (d) ROLD-EPR; (e) DWM; (f) ASWM;(g) RORD-WMF; (h) NSDD; (i) AOP; (j) DFA; (k) FWNLM; (l) SAFE.

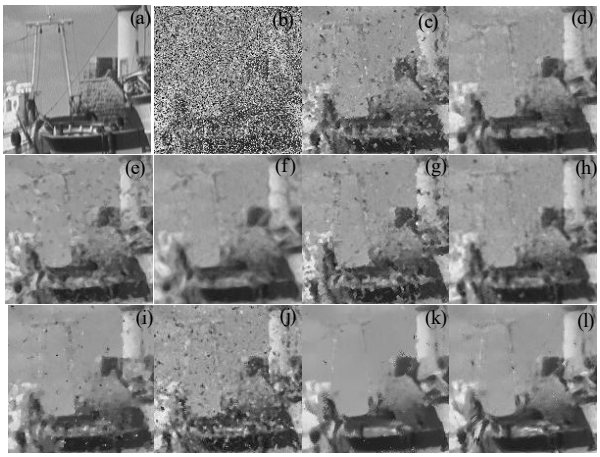

Fig.8. Restoration results for Boat image (60% noise density). (a) Original image; (b) Corrupted image; (c) ACWMF; (d) ROLD-EPR; (e) DWM; (f) ASWM;(g) RORD-WMF; (h) NSDD; (i) AOP; (j) DFA; (k) FWNLM; (l) SAFE.

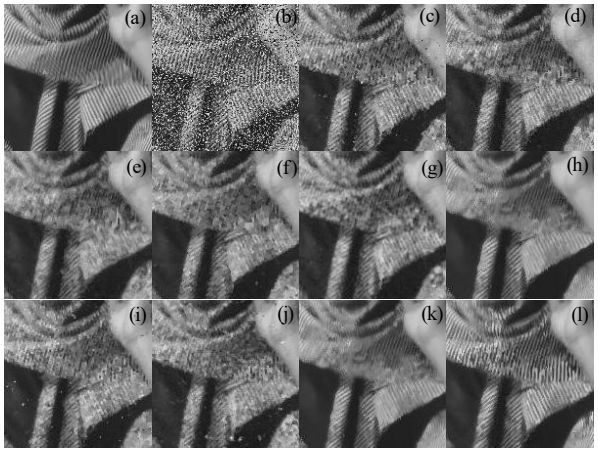

Fig.9. Restoration results for Barbara image (40% noise density). (a) Original image; (b) Corrupted image; (c) ACWMF; (d) ROLD-EPR; (e) DWM; (f) ASWM;(g) RORD-WMF; (h) NSDD; (i) AOP; (j) DFA; (k) FWNLM; (l) SAFE.

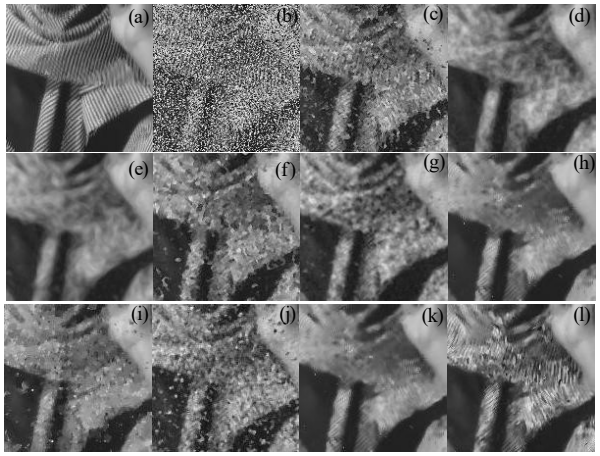

Fig.10. Restoration results of different methods for Barbara image (60% noise

This article has been accepted for publication in a future issue of this journal, but has not been fully edited. Content may change prior to final publication. Citation information: DOI 10.1109/TCSVT.2016.2615444, IEEE Transactions on Circuits and Systems for Video Technology

density). (a) Original image; (b) Corrupted image; (c) ACWMF; (d) ROLD-EPR; (e) DWM; (f) ASWM;(g) RORD-WMF; (h) NSDD; (i) AOP; (j) DFA; (k) FWNLM; (l) SAFE.

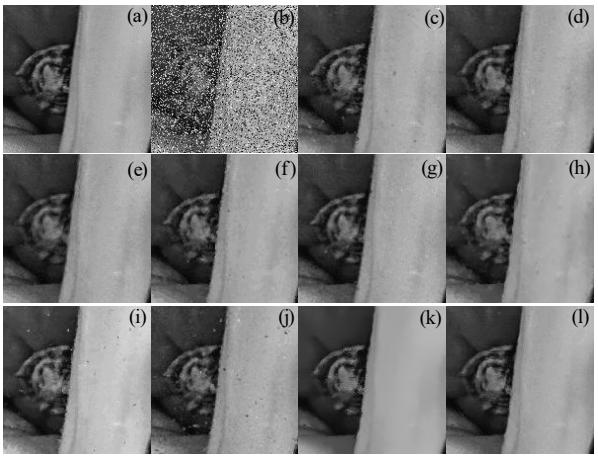

Fig.11. Restoration results of different methods for Peppers image (40% noise density). (a) Original image; (b) Corrupted image; (c) ACWMF; (d) ROLD-EPR; (e) DWM; (f) ASWM;(g) RORD-WMF; (h) NSDD; (i) AOP; (j) DFA; (k) FWNLM; (l) SAFE.

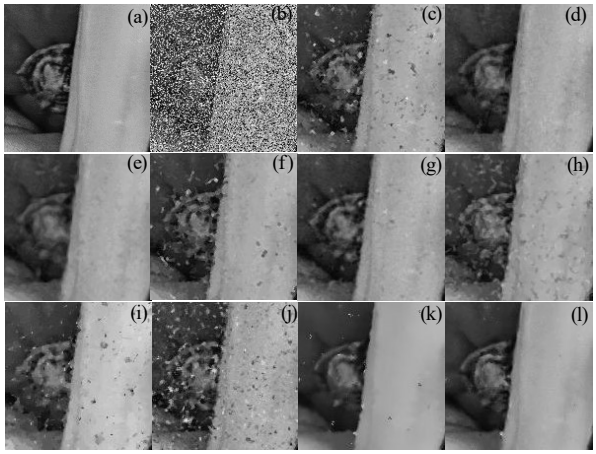

Fig.12. Restoration results of different methods for Peppers image (60% noise density). (a) Original image; (b) Corrupted image; (c) ACWMF; (d) ROLD-EPR; (e) DWM; (f) ASWM;(g) RORD-WMF; (h) NSDD; (i) AOP; (j) DFA; (k) FWNLM; (l) SAFE.

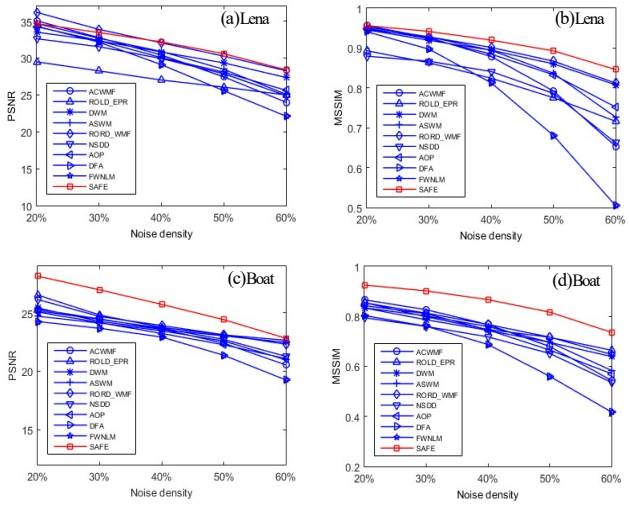

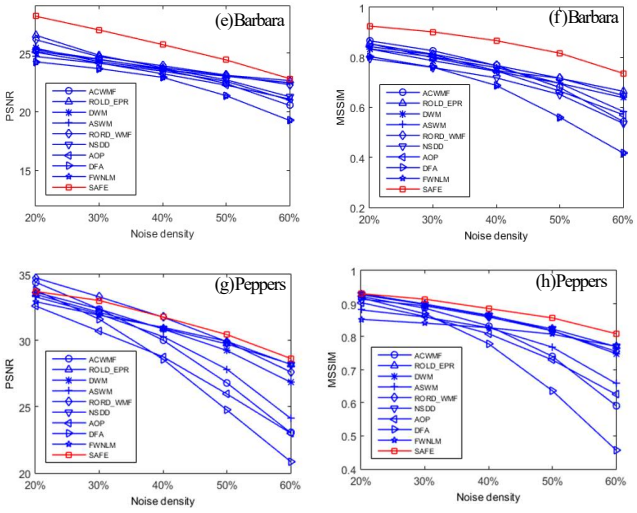

Fig.13. PSNR and MSSIM values for restorations with varying noise densities using different algorithms. (a) and (b): the PSNR and MSSIM for Lena image; (c) and (d): the PSNR and MSSIM for Boat image; (e) and (f): the PSNR and MSSIM for Barbara image; (g) and (h): the PSNR and MSSIM for Peppers image.

C. Validation of the MPSP Based Reliability Metric

We implemented the SAFE algorithm with different binary reliability strategies to show the advantage of the proposed fuzzy reliability. Here, the ACWMF method (denoted by R_BR_ACWMF) is used, and the binary reliability means an explicit classification of pixels into corrupted and non-corrupted points. Different binary reliability maps were produced by hard thresholding the reliability maps R using thresholds ranging from 0.1 to 0.9 (R_BR_0.1 to R_BR_0.9). The parameters in the restoration step were set based on TABLE I to provide a fair evaluation. We plot in Fig.15(a)-(d) the PSNR values of different images restored by the SAFE algorithm using different reliability maps. We can see in Fig.15 that, except for the Boat image with 20% noise density, the proposed MPSP based reliability metric (denoted by R_Fuzzy_MPSP) leads to higher PSNR values than all the binary reliability metrics for all the images.

D. Validation of Recursion Stopping

Fig.14 plots the PSNR with respect to SAFE iterations for the restored Lena image (blue lines) and the PSNR-R of the reliability image information (green lines) under different noise densities. The same parameter set defined above was used for this validation. The iterations with the highest PSNR and PSNR-R values are tagged in red. We can note that the PSNR values decrease after some iterations: this result confirms the deterioration that may occur when applying the SAFE method. A good overall match of the highest values between the true PSNR of the restored images and PSNR-R of the re-estimated pixels can be observed with however a progressive deviation when the noise density increases to 50%. The reason of such match deviation is due to the increased error of the MPSP-based reliability calculation under high noise densities. We can also observe that the PSNR evolution over iterations becomes more and more stable as the noise density increases. Such observation supports the proposed stopping strategy for the SAFE algorithm: the metric PSNR-R is used to control the

This article has been accepted for publication in a future issue of this journal, but has not been fully edited. Content may change prior to final publication. Citation information: DOI 10.1109/TCSVT.2016.2615444, IEEE Transactions on Circuits and Systems for Video Technology

TABLE II
PSNR and MSSIM (IN THE RIGHT BRACKET) FOR DIFFERENT METHODS WITH DIFFERENT NOISE DENSITIES (THE HIGHEST VALUES ARE GIVEN IN BOLD)

	Lena (20% ND)	**Lena (30% ND)**	**Lena (40% ND)**	**Lena (50% ND)**	**Lena (60% ND)**
Noisy image	16.23 (0.1735)	14.49 (0.1155)	13.24 (0.0827)	12.28 (0.0619)	11.49 (0.0459)
ACWMF	35.04 (0.9564)	32.76 (0.9262)	30.39 (0.8788)	27.44 (0.7924)	23.98 (0.6538)
ROLD-EPR	34.84 (0.9500)	32.00 (0.9181)	30.88 (0.8935)	29.65 (0.8590)	28.04 (0.8101)
DWM	33.99 (0.9364)	32.48 (0.9030)	30.97 (0.8832)	29.42 (0.8510)	27.41 (0.8033)
ASWM	34.69 (0.9529)	32.74 (0.9287)	30.67 (0.8934)	28.45 (0.8400)	25.20 (0.7312)
RORD-WMF	**36.18** (0.9462)	**33.79** (0.9277)	32.05 (0.9016)	30.25 (0.8673)	28.27 (0.8123)
NSDD	32.61 (0.8801)	31.30 (0.8535)	29.91 (0.8412)	28.11 (0.7905)	25.73 (0.7146)
AOP	34.23 (0.9494)	32.34 (0.9240)	30.05 (0.8848)	28.07 (0.8331)	25.62 (0.7524)
DFA	34.27 (0.9417)	32.16 (0.8973)	29.16 (0.8143)	25.63 (0.6810)	22.08 (0.5011)
FWNLM	33.685 (0.9133)	32.48 (0.8990)	31.33 (0.8810)	29.96 (0.8555)	28.22 (0.8146)
SAFE	34.65 **(0.9565)**	33.45 **(0.9416)**	**32.18 (0.9199)**	**30.58 (0.8931)**	**28.38 (0.8461)**
	Boat (20% ND)	**Boat (30% ND)**	**Boat (40% ND)**	**Boat (50% ND)**	**Boat (60% ND)**
Noisy image	16.27 (0.2280)	14.54 (0.1569)	13.29 (0.1138)	12.35 (0.0861)	11.55 (0.0632)
ACWMF	30.63 (0.9188)	29.05 (0.8809)	27.26 (0.7805)	25.23 (0.7336)	22.42 (0.5997)
ROLD-EPR	30.42 (0.9159)	28.15 (0.8682)	26.88 (0.8278)	26.04 (0.7811)	24.97 (0.7194)
DWM	29.66 (0.8706)	28.24 (0.8449)	27.07 (0.8108)	25.88 (0.7607)	24.35 (0.6902)
ASWM	30.14 (0.9074)	28.88 (0.8729)	27.33 (0.8252)	25.63 (0.7586)	23.23 (0.6457)
RORD-WMF	**31.34** (0.9120)	**29.26** (0.8836)	27.81 (0.8408)	**26.57** (0.7912)	24.97 (0.7179)
NSDD	28.76 (0.8186)	28.17 (0.7962)	26.70 (0.7616)	25.13 (0.6929)	23.52 (0.6102)
AOP	30.40 (0.9155)	28.80 (0.8738)	27.05 (0.8168)	25.27 (0.7406)	23.27 (0.6470)
DFA	29.83 (0.9045)	28.39 (0.8563)	26.53 (0.7782)	23.97 (0.6542)	20.97 (0.4915)
FWNLM	29.33 (0.8660)	28.18 (0.8366)	27.19 (0.8023)	26.06 (0.7587)	24.92 (0.6916)
SAFE	30.59 **(0.9214)**	28.99 **(0.8911)**	**27.97 (0.8547)**	26.48 **(0.7992)**	**25.08(0.7341)**
	Barbara(20%ND)	**Barbara(30%ND)**	**Barbara(40%ND)**	**Barbara(50%ND)**	**Barbara(60%ND)**
Noisy image	15.81 (0.2646)	14.08 (0.1897)	12.83 (0.1413)	11.88 (0.1064)	11.09 (0.0793)
ACWMF	25.31 (0.8664)	24.48 (0.8266)	23.62 (0.7673)	22.40 (0.6796)	20.54 (0.5442)
ROLD-EPR	25.72 (0.8679)	24.67 (0.8117)	23.74 (0.7634)	23.11 (0.7142)	22.65 (0.6630)
DWM	25.71 (0.8082)	24.40 (0.7657)	23.59 (0.7267)	23.03 (0.7001)	22.48 (0.6419)
ASWM	24.70 (0.8345)	24.17 (0.8026)	23.48 (0.7603)	22.58 (0.6984)	21.01 (0.5843)
RORD-WMF	26.14 (0.8544)	24.70 (0.8129)	23.91 (0.7677)	23.13 (0.7169)	22.31 (0.6477)
NSDD	25.16 (0.8213)	24.73 (0.7695)	23.68 (0.7181)	23.10 (0.6670)	21.90 (0.5804)
AOP	25.07 (0.8433)	24.16 (0.8107)	23.23 (0.7460)	22.27 (0.6654)	21.07 (0.5707)
DFA	24.75 (0.8127)	23.73 (0.7625)	22.94 (0.6899)	21.44 (0.5694)	19.28 (0.4157)
FWNLM	27.66 (0.8996)	26.24 (0.8634)	25.11 (0.8165)	24.13 (0.7587)	**23.10** (0.6868)
SAFE	**28.14 (0.9254)**	**26.97 (0.9020)**	**25.72 (0.8668)**	**24.41 (0.8169)**	22.82 **(0.7362)**
	Peppers(20% ND)	**Peppers(30% ND)**	**Peppers(40% ND)**	**Peppers(50% ND)**	**Peppers(60% ND)**
Noisy image	15.86 (0.1693)	14.11 (0.1118)	12.86 (0.0800)	11.91 (0.0595)	11.12 (0.0450)
ACWMF	34.41 (0.9214)	32.39 (0.8863)	30.03 (0.8328)	26.81 (0.7409)	23.04 (0.5917)
ROLD-EPR	33.50 (0.9266)	32.13 (0.8975)	30.92 (0.8635)	29.75 (0.8235)	28.22 (0.7701)
DWM	33.65 (0.9306)	32.38 (0.8988)	30.87 (0.8649)	29.25 (0.8181)	26.85 (0.7489)
ASWM	33.31 (0.8811)	32.00 (0.8596)	30.30 (0.8276)	27.84 (0.7684)	24.13 (0.6587)
RORD-WMF	**34.76** (0.9135)	**33.31** (0.8935)	31.77 (0.8597)	29.92 (0.8176)	27.64 (0.7559)
NSDD	33.50 (0.9266)	32.13 (0.8976)	30.92 (0.8635)	29.75 (0.8235)	28.22 (0.7701)
AOP	32.62 (0.9030)	30.70 (0.8612)	28.78 (0.8092)	25.97 (0.7301)	23.01 (0.6257)
DFA	33.81 (0.9175)	31.61 (0.8694)	28.59 (0.7780)	24.76 (0.6369)	20.86 (0.4575)
FWNLM	32.94 (0.8526)	31.92 (0.8411)	31.00 (0.8273)	29.95 (0.8078)	28.20 (0.7708)
SAFE	33.72 **(0.9302)**	33.03 **(0.9136)**	**31.78 (0.8852)**	**30.46 (0.8569)**	**28.65 (0.8092)**

TABLE III
COMPUTATION COST (IN SECONDS) FOR DIFFERENT METHODS WITH DIFFERENT NOISE DENSITIES (ND)

	Lena (20% ND)	**Lena (30% ND)**	**Lena (40% ND)**	**Lena (50% ND)**	**Lena (60% ND)**
ACWMF	20.3893	19.5625	19.3285	19.5625	19.1413
ROLD-EPR	12.9637	17.2381	17.7217	20.8729	34.8974
DWM	122.0396	122.6948	138.1077	155.3146	183.8316
ASWM	51.8391	54.8344	58.8436	62.3692	66.1288
RORD-WMF	0.3276	1.1076	1.2636	1.1856	1.2636
NSDD	35.1314	34.5542	34.2890	33.4778	32.6510
AOP	8.9389	10.2181	12.2305	14.4613	16.8793
DFA	18.7669	17.7825	19.2505	18.9697	19.6405
FWNLM	994.4752	993.49241	992.8216	994.2100	994.1008
Un-parallelized SAFE	768.0553	763.4845	759.5377	753.5004	749.6160
SAFE	11.3725	13.1041	12.7453	14.4765	16.2085

This article has been accepted for publication in a future issue of this journal, but has not been fully edited. Content may change prior to final publication. Citation information: DOI 10.1109/TCSVT.2016.2615444, IEEE Transactions on Circuits and Systems for Video Technology

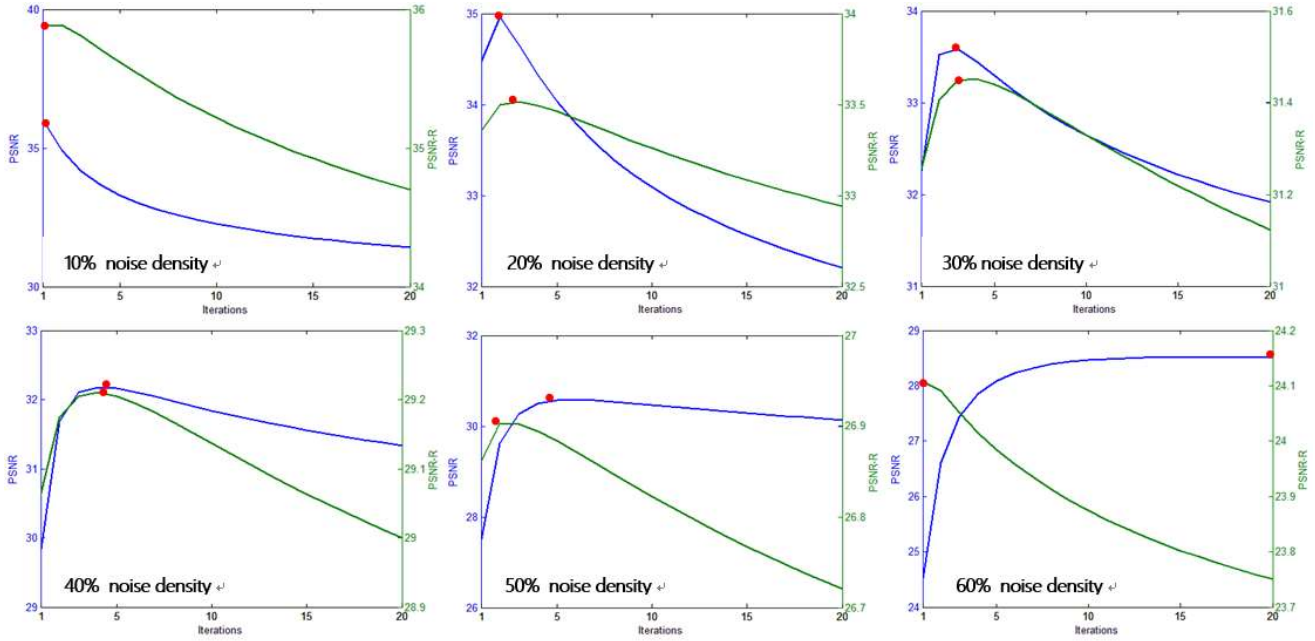

Fig.14. PSNR and PSNR-R values for Lena image with various noise densities (from 10% to 60%).

Iteration number when the noise density does not increase over 40% while the normed difference between two consecutive iterated images is used otherwise.

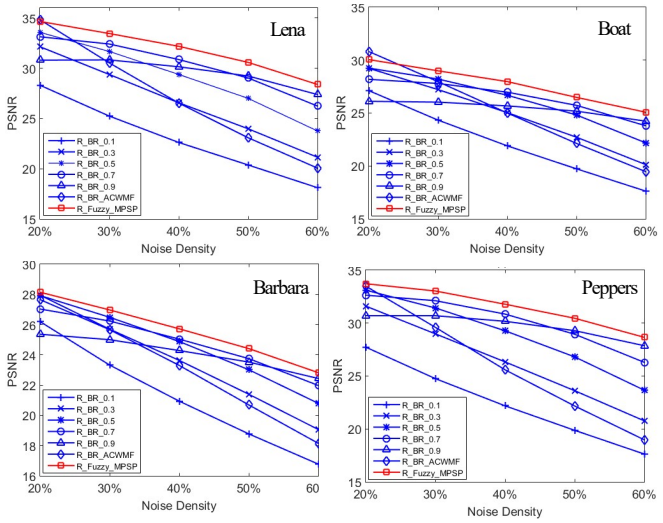

Fig.15. Comparison of the proposed MPSP based reliability metric with binary reliability metric in the SAFE restoration

E. Computational Complexity

TABLE III lists the computation costs (in seconds) in implementing all the methods in the above experiments with different noise densities. The RORD-WMF method appears as the fastest one and the un-parallelized SAFE is the most expensive. TABLE III also shows that the GPU based implementation leads to a significant acceleration (from 35 to 70 times) of the original un-parallelized SAFE processing. The computation costs for the SAFE approach increase with the noise density due to the fact that more iterations of the intensity re-estimation are required to meet the stopping criterion. The feasibility of the SAFE method using a parallelization technique is however demonstrated.

IV. CONCLUSION

This paper has proposed an iterative fuzzy approach named SAFE to remove random-valued impulse noise under the frame of Gaussian Maximum Likelihood Estimation. Image structure information is effectively incorporated to determine the two fuzzy metrics of reliability and similarity. In particular, a novel membership function on pixel reliability has been designed based on the Minimal Path Based Structure Propagation (MPSP) providing a structure-adaptive evaluation of point reliability. The restoration quality is iteratively refined and the total iteration number can be well controlled by the re-estimated reliability information. The experiments conducted on several images with different noise densities demonstrate that the proposed SAFE method has a good performance in both noise suppression and structure restoration when compared to other methods, especially for high noise densities. Another merit is that the SAFE method is robust to parameter setting, *i.e.* the same parameter set can be used in processing all the test images.

The results in Fig.15 show that the binary noise detection step in ACWMF method can lead to higher PSNR than the proposed fuzzy reliability metrics under low noise densities. We can further improve the estimation of the reliability metric by using a multi-sized window strategy in the ACWMF method. Another issue concerns the fact that the accuracy of the MPSP estimation decreases as the noise density increases. Therefore, a better restoration can be expected by designing a new fuzzy reliability metric adaptively estimated according to different noise levels. Currently, a constant smoothing parameter h (in Eq. (7)) is used in the SAFE algorithm and a further

improvement may be obtained by optimizing this parameter as pointed out in [52] and [53]. A more thorough analysis on issues such as the window size, different fuzzy member function models and clustering stability will also be considered. In addition, though parallelized by means of a GPU technique, the proposed SAFE still needs a further acceleration for real-time processing tasks. Future work will be devoted to addressing the above problems.

ACKNOWLEDGEMENTS

The authors would like to thank anonymous reviewers for giving valuable comments on this paper.

REFERENCES

[1] A. Bovik, Handbook of Image and Video Processing. New York: Academic, 2000.

[2] J. Astola and P. Kuosmaneen*, Fundamentals of Nonlinear Digital Filtering*. Boca Raton, FL: CRC, 1997.

[3] T. Chen and H. R.Wu, "Space variant median filters for the restoration of impulse noise corrupted images," *IEEE Trans on Circuit and System -II*, vol. 48, no. 8, pp. 784-789, 2001.

[4] R. H. Chan, C.-W. Ho, and M. Nikolova, "Salt and pepper noise removal by median type noise detectors and detail preserving regularization," *IEEE Trans. Image Process.*, vol. 14, no. 10, pp. 1479-1485, 2005.

[5] P. Sree, P. Kumar, R. Siddavatam, R. Verma, "Salt-and-pepper noise removal by adaptive median-based lifting filter using second-generation wavelets," *Signal, Image and Video Processing*, vol. 7, no. 1, pp. 111-118, 2013.

[6] Z. Wang and D. Zhang, "Progressive switching median filter for the removal of impulse noise from highly corrupted images," *IEEE Trans on Circuit and System-II*, vol. 46, no. 1, pp. 78-80, Jan. 1999.

[7] H. L. Eng and K.-K. Ma, "Noise adaptive soft-switching median filter, " *IEEE Trans. Image Process.*, vol. 10, no. 2, pp. 242-251, 2001.

[8] P. E. Ng and K. K. Ma, "A switching median filter with boundary discriminative noise detection for extremely corrupted images," *IEEE Trans. Image Process*., vol. 15, no. 6, pp. 1506-1516, 2006.

[9] M. Yildirim, A. Basturk, M. Yuksel, "Impulse noise removal from digital images by a detail-preserving filter based on type-2 fuzzy logic," *IEEE Trans on Fuzzy Systems*, vol. 16, no. 4, pp. 920-928, 2008.

[10] T. Chen, H.R. Wu, "Adaptive impulse detection using center-weighted median filters," *IEEE Signal Processing Letters*., vol.8, no.1, pp. 1-3, 2001

[11] R.H. Chan, C. Hu, M. Nikolova, "An iterative procedure for removing random-valued impulse noise," *IEEE Signal Process. Lett*., 11, pp. 921-924, 2004.

[12] J. J. Zhang, "An efficient median filter based method for removing random-valued impulse noise," *Digital Signal Processing*., vol. 20, no. 4, pp. 1010-1018, 2010.

[13] J. Jiang, L. Zhang, and J. Yang, "Mixed noise removal by weighted encoding with sparse nonlocal regularization," *IEEE Trans. Image Process*., vol.23, no.6, pp.2651-2662,2014.

[14] S. Zhang and M. A. Karim, "A new impulse detector for switching median filters," *IEEE Signal Process. Lett*., vol. 9, no. 11, pp. 360-363, 2002.

[15] I. Aizenberg, C. Butakoff, "Effective impulse detector based on rank-order criteria," *IEEE Signal Process. Lett*., vol.11, no.3, pp. 363-366, 2004.

[16] R. Garnett, T. Huegerich, C. Chui, and W.-J. He, "A universal noise removal algorithm with an impulse detector," *IEEE Trans. Image Process*., vol. 14, no. 11, pp. 1747-1754, 2005.

[17] Y. Q. Dong, R. H. Chan and S. F Xu, "A detection statistic for random-valued impulse noise," *IEEE Trans. Image Process*., vol. 16, no. 4, pp. 1112-1120, 2007.

[18] Y. Q. Dong, and S. F Xu, "A new directional weighted median filtering for removal of random-valued impulse noise," *IEEE Signal Process. Lett*., vol. 14, no. 3, pp. 193-196, 2007.

[19] H. Yu, L. Zhao, H. Wang. "An efficient procedure for removing random-valued impulse noise in images," *IEEE Signal Process Lett*., vol. 15, pp. 922-925, 2008.

[20] X. M. Zhang and Y. L. Xiong, "Impulse noise removal using directional difference based noise detector and adaptive weighted mean filter," *IEEE Signal Process. Lett.,* vol. 16, no. 4, pp. 295–298, 2009.

[21] S. Akkoul, R. Ledee, R. Leconge and R. Harba, "A new adaptive switching median filter," *IEEE Signal Process. Lett*., vol. 17, no. 6, pp. 587-590, 2010.

[22] J. Wu and C. Tang, "PDE-Based Random-Valued Impulse Noise Removal Based on New Class of Controlling Functions," *IEEE Trans. Image Process*., vol. 20, no. 9, pp. 2028-2039, 2011.

[23] M. Yan, "Restoration of images corrupted by impulse noise and mixed Gaussian impulse noise using blind inpainting," *SIAM Journal on Imaging Sciences*, vol. 6, no. 3, pp.1227-1245, 2013

[24] C.S. Lee, Y.H. Kuo, P.T. Yu, "Weighted fuzzy mean filters for image processing," *Fuzzy Sets and Systems*., vol. 89, no. 2, pp. 157-180, 1997.

[25] M. Mancuso, R. D. Luca, R. Poluzzi, G. G. Rizzotto, "A fuzzy decision directed filter for impulsive noise reduction," *Fuzzy Sets and Systems*., vol. 77, no. 1, pp. 111-116, 1996.

[26] H. Xu, G. Zhu, H. Peng, D. Wang, "Adaptive fuzzy switching filter for images corrupted by impulse noise," *Pattern Recognition Letters*., vol. 25, no. 15, pp. 1657-1663, 2004.

[27] C. S. Lee, S. M. Guo, C.Y. Hsu, "Genetic-based fuzzy image filter and its application to image processing," *IEEE Trans. Syst, Man, and Cybern*., vol. 35, no. 4, 694-711, 2005.

[28] A. Toprak, İ. Güler, "Impulse noise reduction in medical images with the use of switch mode fuzzy adaptive median filter," *Digital Signal Processing*., vol. 17, no. 4, pp. 711-723, 2007

[29] W. Luo, "An efficient detail-preserving approach for removing impulse noise in images," *IEEE Signal Process Lett*., vol. 13, no. 7, pp. 413-416, 2006

[30] C. C. Kang, W. J. Wang, "Fuzzy reasoning-based directional median filter design," *Signal Processing*, vol. 89, no. 3, pp. 344-351, 2009

[31] S. Schulte, M. Nachtegael, V. De Witte, D. Van der Weken, E. E. Kerre, "A fuzzy impulse noise detection and reduction method," *IEEE Trans. Image Process*., vol. 15, no. 5, pp. 1153-1162, 2006.

[32] S. Schulte, V. De Witte, M. Nachtegael, D. Van der Weken, E. E. Kerre, "Fuzzy random impulse noise reduction method," *Fuzzy Sets and Systems*., vol. 158, no. 3, pp. 270-283, 2007.

[33] H. C. Chen, W. J. Wang, "Efficient impulse noise reduction via local directional gradients and fuzzy logic," *Fuzzy Sets and Systems*., vol. 160, no. 13, pp. 1841-1857, 2009.

[34] J. G. Camarena, V. Gregori, S. Morillas, et al, "Fast detection and removal of impulsive noise using peer groups and fuzzy metrics," *Journal of Visual Communication and Image Representation.*, vol. 19, no. 1, pp. 20-29, 2008.

[35] J. G. Camarena, V. Gregori, S. Morillas, et al, "Some improvements for image filtering using peer group techniques," *Image and Vision Computing.*, vol. 28, no. 1, pp. 188-201, 2010.

[36] T. C. Lin, "Decision-based fuzzy image restoration for noise reduction based on evidence theory," *Expert Systems with Applications*., vol. 38, no. 7: 8303-8310, 2011.

[37] W. Jian and T. Chen, "Random-valued impulse noise removal using fuzzy weighted non-local means", *Signal, Image and Video Processing*, vol. 8, no. 2, pp 349-355, 2014.

[38] Justusson, B. I."Median filtering: Statistical

properties." *Two-Dimensional Digital Signal Processing-II*. Springer Berlin Heidelberg, pp. 161-196, 1981.

[39] G. R. Arce, "A general weighted median filter structure admitting negative weights," *IEEE Trans. Signal Process.*, vol. 46, no. 12, pp. 3195-3205, 1998.

[40] J. W. Harris, and H. Stocker, "Maximum Likelihood Method." (§21.10.4) in Handbook of Mathematics and Computational Science. New York: Springer-Verlag, pp. 824, 1998.

[41] Y. Chen, J. Yang, H. Shu, L. Shi, J. Wu, et al., "2-D impulse noise suppression by recursive Gaussian maximum likelihood estimation," *PLoS ONE* vol.9, no.5, pp e96386, 2014.

[42] A. Buades, B. Coll, J. M. Morel. "A non-local algorithm for image denoising," 2005 *IEEE Computer Vision and Pattern Recognition*, vol.2, pp. 60-65, 2005.

[43] Y. Chen, L.M Luo, W.F Chen et al, "Nonlocal Prior Bayesian Tomographic Reconstruction," *Journal of Mathematical Imaging and Vision*, vol. 30, no. 2, pp.133-146, 2008.

[44] Y. Chen, L.M Luo, W.F Chen et al, "Joint-MAP tomographic reconstruction with patch similarity based mixture prior model," *Multiscale Modeling and Simulation*, vol. 9, no. 4, pp. 1399-1419, 2011.

[45] L.D. Cohen and R. Kimmel, "Global Minimum for Active Contour Models: A Minimal Path Approach," *International Journal of Computer Vision*, vol. 24, no. 1, pp. 57-78, 1997.

[46] O. Wink, W. Niessen, and M. Viergever, "Multiscale vessel tracking," *IEEE Trans. Med. Image.*, vol. 23, no. 1, pp. 130–133, Jan. 2004.

[47] Y. Chen, Y. Zhang, J. Yang, Q. Cao, G. Yang, J. Chen, H. Shu, L. Luo, J-L Coatrieux, Qianjing Feng. "Curve-like Structure Extraction Using Minimal Path Propagation with Backtracking," *IEEE Trans. Image Process.*, vol. 25, no. 2, pp. 988-1003, 2016

[48] J. A. Hartigan and M. A. Wong "A K-Means Clustering Algorithm", *Journal of the Royal Statistical Society.Series C(Applied Statistics)*, vol. 28, no. 1, pp.100-108, 1979

[49] NVIDIA CUDATM Programming Guide (Version 3.0), http://developer.download.nvidia.com/compute/cuda/3.0/toolkit/docs/NVIDIA CUDA Programming Guide.pdf.

[50] Accelerating MATLAB with CUDA Using MEX Files (White Paper), http://developer.nvidia.com/object/matlab cuda.html.

[51] Z. Wang, Alan C. Bovik, Hamid R. Sheikh and Eero P. Simoncelli "Image quality assessment: from error visibility to structural similarity" *IEEE Trans. Image Process*, vol. 13, no. 4, pp. 600-612, 2004.

[52] C. -A. Deledalle, L. Denis, F. Tupin, "Iterative weighted maximum likelihood denoising with probabilistic patch-based weights," *IEEE Trans. Image Process.*, vol. 18, no. 12, pp.2661-2672, 2009

[53] D. Van De Ville and M. Kocher, "Nonlocal means with dimensionality reduction and SURE-based parameter selection," *IEEE Trans. Image Process.*, vol. 20, no. 9, pp. 2683-2690, 2011.

This article has been accepted for publication in a future issue of this journal, but has not been fully edited. Content may change prior to final publication. Citation information: DOI 10.1109/TCSVT.2016.2615444, IEEE Transactions on Circuits and Systems for Video Technology

Response to Comments

Dear Editor and reviewers:

We appreciated the comments made on our paper. They allowed us clarifying, improving and completing our work. We revised the paper carefully based on each comment, and invited an English professor to give a thorough checking of the language through the paper. Points by point replies are provided below and the revised version has been changed accordingly. The responses are written in blue color under the corresponding original comments.

Reviewer(s)' Comments to Author:

Control Number: 10535
Title: Structure-adaptive Fuzzy Estimation for Random-Valued Impulse Noise Suppression
Authors: yang chen ; jian yang ; huazhong shu ; limin luo ; Jean-Louis Coatrieux ; qianjing feng

We have completed the review process of the above referenced paper for the IEEE Transactions on Circuits and Systems for Video Technology. Based on the reviewers' comments, we recommend that your paper undergo a Minor Revision and be resubmitted for consideration by the reviewers.

Title: Structure-adaptive Fuzzy Estimation for Random-Valued Impulse Noise Suppression
Authors: yang chen ; jian yang ; huazhong shu ; limin luo ; Jean-Louis Coatrieux ; qianjing feng

Reviewers' and Associate Editor's Comments
==========

Review Number 1.
****

Does the revision adequately address the concerns expressed in the original review?

Partially.

Comments to the Author

My major concern is not about technical part, but the writing of this paper. The authors have to improve the paper writing. There are so many grammar errors in the paper. Quick examples are (there are more)
1) In "A2: neighboring pixels belonging to the structure similar as the current point should be considered with a higher possibility of belonging to the same structure, and should be assigned a low variance in estimating the current pixel in Eq. (4). ", "similar as" should be "similar to"
2) In "Note such subscript rule also applies to other denotations in this paper", "denotations" should be "notations"
3) The authors keep using "possibility " in the whole paper. It should be "probability".
4) In "in each propagation window. these two paths being linked together.", this is not a complete sentence.
Response: we addressed all the above points in the revised paper

I strongly encourage the authors to ask a native English speaker to assist you with editing. There are also some minor concerns.
Response: we have invited a professor friend of us to give a thorough language checking of the revised paper

1) Please double check Fig. 10 and 11. In Fig. 10, (a) is the original image, but according to the figure, it seems (e) is the original figure. The same problem exists in Fig. 11 that (b) should be the original image instead of (a).
Response: very sorry for these errors, which were induced in reformatting the paper into one with less pages. We have carefully checked all the paper to correct them.

2) Please reorganize Fig. 5 "SAFE Algorithm Outline ". The layout does not look good. Moreover, "SAFE Algorithm Outline " and "Outline of Algorithm MPSP" should not be named as Fig.4 and 5. If possible, please use latex for future submission instead of MS word.
Response: The outlines have been reformatted to avoid confusion with figures, and we agree that latex should be used in our future work.

Review Number 2.
****

Comments to the Author

Some of the typos mentioned in the previous review are not corrected. Repeating them here,

1) page 4 . Right after fig1. "We illustrate in Fig.1(a) the tracked minimal paths for eightuncorrupted points, and Fig.1(b) the results for eight uncorrupted ones." fig1(b) are corrupted points.

2) Figure 3. Top-row : Spelling mistake in the legend in the figure. It should be 'Corrupted'. Not 'Currupted'.

The paper looks good otherwise.
Response: Sorry for this repetitive errors, and we carefully checked the paper to correct them.